ACSNANO

www.acsnano.org

ARTICLE

Evolution of Plasmonic Metamolecule Modes in the Quantum Tunneling Regime

Jonathan A. Scholl,[†,⊥] Aitzol Garcia-Etxarri,[*,†,‡,⊥] Garikoitz Aguirregabiria,[‡] Ruben Esteban,[‡] Tarun C. Narayan,[†] Ai Leen Koh,[§] Javier Aizpurua,[‡] and Jennifer A. Dionne[*,†,∥]

[†]Department of Materials Science and Engineering, Stanford University, Stanford, California 94305, United States

[‡]Center for Material Physics, CSIC - UPV/EHU and DIPC, Donostia, San Sebastian 20018, Spain

[§]Stanford Nanocharacterization Laboratory, Stanford University, Stanford, California 94305, United States

[∥]Stanford Institute for Materials and Energy Sciences, SLAC National Accelerator Laboratory, 2575 Sand Hill Road, Menlo Park, California 94025, United States

S *Supporting Information*

ABSTRACT: **Plasmonic multinanoparticle systems exhibit collective electric and magnetic resonances that are fundamental for the development of state-of-the-art optical nanoantennas, metamaterials, and surface-enhanced spectroscopy substrates. While electric dipolar modes have been investigated in both the classical and quantum realm, little attention has been given to magnetic and other "dark" modes at the smallest dimensions. Here, we study the collective electric, magnetic, and dark modes of colloidally synthesized silver nanosphere trimers with varying interparticle separation using scanning transmission electron microscopy (STEM) and electron energy-loss spectroscopy (EELS). This technique enables direct visualization and spatially selective excitation of individual trimers, as well as manipulation of the interparticle distance into the subnanometer regime with the electron beam. Our experiments reveal that bonding electric and magnetic modes are significantly impacted by quantum effects, exhibiting a relative blueshift and reduced EELS amplitude compared to classical predictions. In contrast, the trimer's electric dark mode is not affected by quantum tunneling for even Ångström-scale interparticle separations. We employ a quantum-corrected model to simulate the effect of electron tunneling in the trimer which shows excellent agreement with experimental results. This understanding of classical and quantum-influenced hybridized modes may impact the development of future quantum plasmonic materials and devices, including Fano-like molecular sensors and quantum metamaterials.**

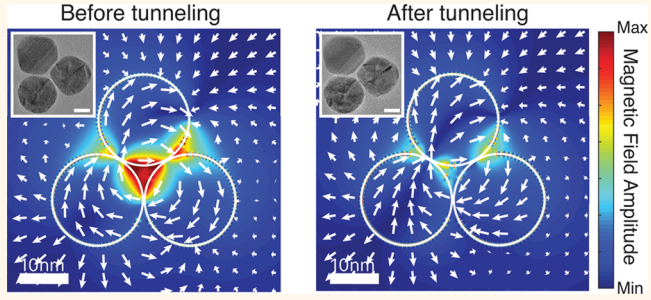

KEYWORDS: *plasmon, nanoparticle, quantum tunneling, electron energy-loss spectroscopy, quantum-corrected model*

Noble metal nanoparticles have attracted substantial interest in recent years owing to their ability to support localized surface plasmon resonances (collective oscillations of conduction electrons). These plasmonic excitations allow manipulation of light at the nanoscale and have enabled technological advances ranging from improved catalytic and photovoltaic cell efficiencies[1−3] to sensitive molecular detectors,[4−6] medical therapeutics,[7,8] nanoscale lasers,[9] spasers,[10] and modulators.[11]

While most plasmonic systems have been designed using a classical electrodynamic framework, several recent studies have shown that quantum effects can significantly modify the electromagnetic response.[12−21] For example, quantum phenomena such as tunneling and size-dependent confinement effects have been observed, leading to relative blueshifts and resonance quenching,[12,14−16] as well as the emergence of new tunneling modes.[17] These results not only provide an important design consideration for optical nanoantennas,[19,22−24] but may also enable ultrafine sensors[25] and new molecular electronic devices.[17]

To date, nearly all studies of quantum plasmonic systems have focused on electric dipolar modes, as are excited in one or two particle systems. Nevertheless, higher-order modes such as magnetic and dark modes are also of paramount importance in plasmonic materials and devices. For example, optical-frequency magnetic resonances have been shown to improve the sensitivity of circular dichroism spectroscopy[26,27] as well as enable tunable permeabilities for novel metamaterials.[28−32] Dark modes (plasmonic resonances that cannot be directly

Received: October 26, 2015
Accepted: December 5, 2015
Published: December 5, 2015

DOI: 10.1021/acsnano.5b06738
ACS Nano 2016, 10, 1346−1354

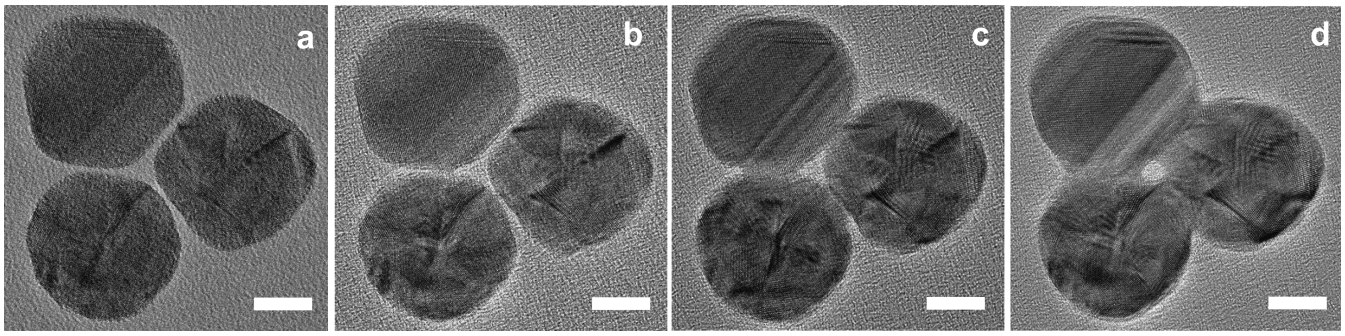

Figure 1. Aberration-corrected TEM images of a silver nanosphere trimer with particles converging and coalescing under the influence of the electron beam. The particles are 25 nm in diameter and supported on an 8 nm-thick SiO_2 membrane substrate. The electron beam induces particle convergence from a separation of 1 nm (a) down through subnanometer gaps (b) until particle contact (c) and ultimate recrystallization into a single entity (d). Scale bars equal 10 nm.

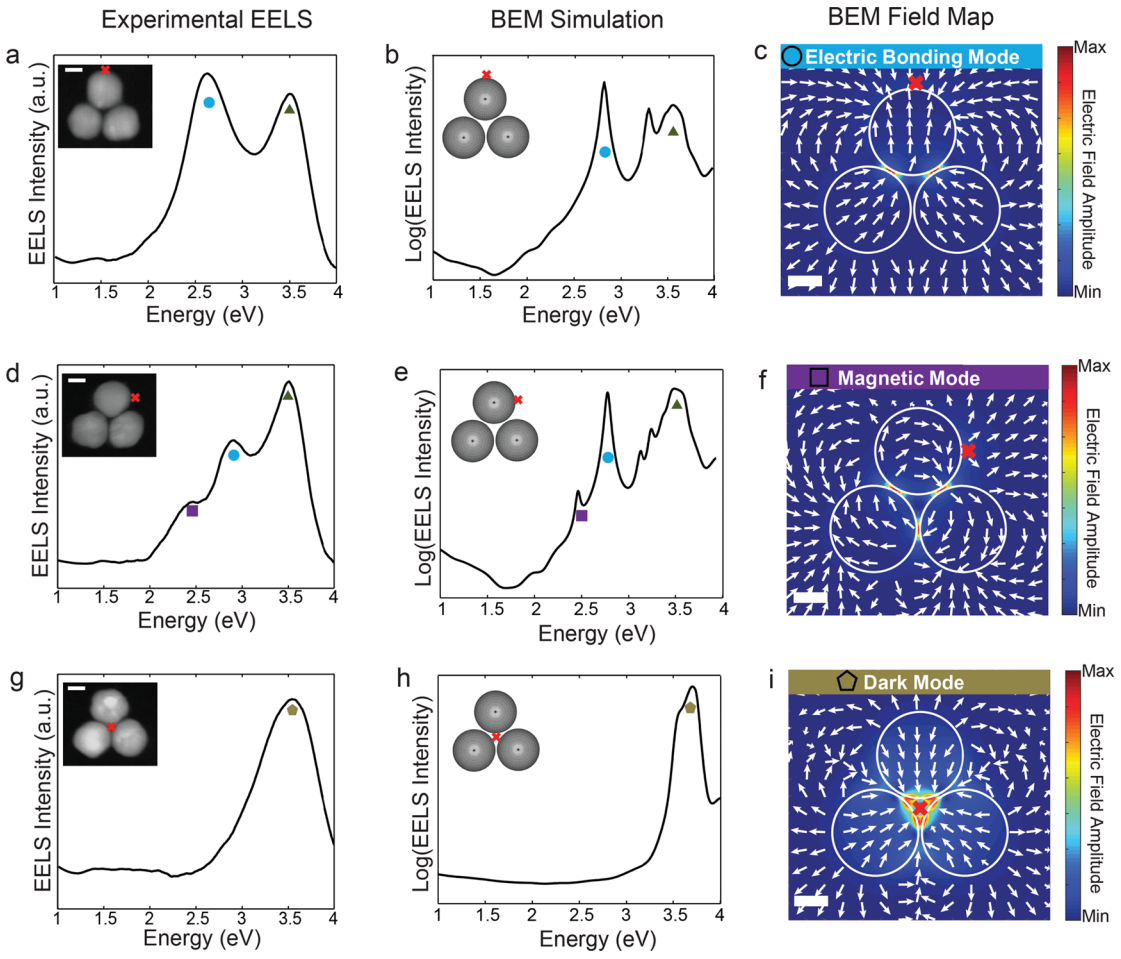

Figure 2. Classical-regime experimental and simulated trimer spectra with field maps for three electron beam excitation positions. Trimers with vertex (a–c), edge (d–f), and center (g–i) excitations (beam position indicated with red X's) are depicted with their experimental STEM-EELS (a, d, and g) and BEM simulation spectra (b, e, and h). The nature of the resonance peak modes is identified with classical BEM field maps and arrows depicting a time snapshot of field direction (c, f, and i). The prominent resonances include electric bonding (blue circle), magnetic (purple square), higher-order modes (green triangle), and dark modes (gold pentagon). All scale bars equal 10 nm.

excited by paraxial light owing to their lack of a net dipole moment) are also of interest in the development of ultrasensitive molecular detectors.[33,34] The influence of quantum effects on these modes remains unexplored, largely due to the challenges associated with fabricating subnanometer features in complex nanoparticle geometries.[35,36]

In this article, we investigate electric, magnetic, and dark plasmonic modes as they transition from the classical to quantum regime. We focus our study on nanoparticle trimers as one of the most basic plasmonic metamolecules supporting a rich variety of resonances of different fundamental character.[33,35,37−40] To access the quantum regime, we use a combination of scanning transmission electron microscopy (STEM) and electron energy-loss spectroscopy (EELS). The focused electron beam is used both to image and manipulate the interparticle separation of self-assembled trimers. Con-

DOI: 10.1021/acsnano.5b06738
ACS Nano 2016, 10, 1346−1354

currently, EELS allows direct probing of the plasmonic response. By correlating plasmonic spectra with trimer geometry, we discover prominent quantum influences on the electric and magnetic modes of trimers at the smallest separation distances but purely classical behavior for the radially symmetric dark mode.

RESULTS AND DISCUSSION

Silver nanospheres are chosen as the constituents of the trimer owing to their strong electric polarizability and capacity to strongly couple. These properties enable the formation of distinct modes with relatively narrow spectral line widths. While smaller particles are more responsive to electron beam manipulation,[41] the nanospheres must also be sufficiently large to exhibit a detectable plasmonic magnetic mode EELS signal. Consequently, 25 nm-diameter particles are selected for this study and synthesized according to a previously reported[42] colloidal chemistry procedure.

The cleaned, concentrated and filtered nanoparticle solution is dropcast on 8 nm thick SiO_2 TEM membranes for analysis. During the process, particles self-assemble on the surface into multimer clusters with varying number of nanosphere constituents, including the equilateral triangle trimers that are the focus of this study.

The nanosphere trimers are imaged and characterized through STEM-EELS, which has the advantages of allowing direct visualization of the individual nanostructures and enabling the selective excitation of plasmonic modes through the placement of the electron beam.[12,43,44] For the purpose of this study, we employ a spherical aberration (Cs) image-corrected FEI Titan TEM with an imaging resolution of 0.07 nm in 300 kV TEM mode. STEM-EELS is performed in 80 kV mode to increase the nanoparticle scattering cross section and improve the spectral energy resolution to 0.1 eV when combined with a monochromator. The focused probe has a spatial resolution of 0.5 nm.

The focused electron beam can be used to induce particle motion, allowing dynamic modification of the interparticle separation. This phenomenon is likely a combination of Coulombic attraction and surface diffusion; the electron beam can induce polarization of the particles into aligned, attractive dipoles[41,45] as well as facilitate the diffusive movement of the nanoparticles' surface atoms.[46−49] The electron-beam-induced merging phenomenon is illustrated in Figure 1, where a series of silver nanosphere trimer TEM images depict decreasing interparticle separation distances. Initially, the 25 nm-diameter spheres self-assemble into an equilateral triangle trimer with gap sizes of ∼1 nm (Figure 1a). After interaction with a focused electron beam, the particles proceed to converge and achieve Ångström-scale separations (Figure 1b). Upon further coalescence, physical connections are established (Figure 1c), which ultimately broaden and recrystallize to create fully merged aggregates (Figure 1d). This final form remains relatively stable and is no longer substantially affected by the electron beam.

Before exploring the modal evolution as the particles coalesce, a baseline understanding of the trimer's plasmonic response to electron excitation is needed for the classical regime (≥0.5 nm gap sizes). As previous EELS work on multimers has been limited,[50−52] we performed fully rigorous three-dimensional Boundary Element Method (BEM) simulations[53−55] (see Methods) to determine which relative electron beam positions would most clearly reveal the trimer's fundamental resonant modes. These classical electrodynamic calculations indicate that electric bonding, magnetic, and dark modes can be excited and detected with the focused beam at the trimer vertex, edge, and center, respectively. These locations are illustrated in Figure 2 along with the experimental and simulated spectral response.

The experimental data in Figure 2 depict the aligned and summed spectra from ≥800 EELS collections, each lasting 10 ms. As a first example of trimer excitation, the vertex position STEM-EELS experimental data is depicted in Figure 2a. The plot features two primary resonance peaks at 2.6 eV (blue circle) and 3.5 eV (green triangle), showing excellent agreement with the simulations of Figure 2b. Note that the SiO_2 substrate used in the experiment causes the resonances to redshift compared to the simulations, which are performed in vacuum. Further, since our theoretical simulations assume a perfectly monochromated electron beam, while the experimental spectra have a small, ∼0.1 eV energy spread in the incident electrons, the experimental spectra show broader resonances than the theory.

To discern the specific nature of the observed plasmonic resonances, simulated field maps are generated for energies corresponding to the spectral peaks. The field maps are accompanied by arrows depicting the direction of the electric field at a given time snapshot. All of the arrows are normalized to have the same length in three dimensions; accordingly, smaller arrows indicate the presence of out-of-plane field components. As seen in Figure 2c, the lower energy resonance of Figure 2b can primarily be attributed to the electric bonding mode in which the field directions exhibit a dominant vertical component. This field geometry indicates a strong dipole coupling similar to the bonding dipolar plasmon resonance of dimers.[14] The two higher energy peaks (>3.4 eV) in the simulation correspond to a more complex combination of higher-order modes, as illustrated in Supporting Information Figure 1.

A second trimer system with edge excitation is presented in Figure 2d. As with the vertex excitation of Figure 2a, electric bonding (blue circle) and higher-order modes (green triangle) are observed, but unlike the vertex excitation, a third, weaker resonance at lower energy (purple square) emerges. This feature, appearing as a shoulder to the electric bonding mode, again shows good correspondence to the idealized theoretical simulations (Figure 2e) that indicate a lower intensity third peak. According to simulated field maps at this energy (Figure 2f), this resonance corresponds to a magnetic mode associated with circulating displacement currents across the three-particle loop.

In Figure 2g, the third excitation position at the trimer's center reveals a unique STEM-EELS resonance profile containing a primary, intense peak at 3.5 eV (gold pentagon). With close correspondence to the classical theoretical simulation (Figure 2h), this resonance indicates the presence of an in-plane, radially symmetric dark mode in which all induced dipoles are directed toward the center (Figure 2i). As the polarization of the individual particles in the trimer create zero net dipole moment, this mode is not excitable with paraxial light.[33] It can, however, be accessed by judicious placement of the electron beam.

With this understanding of the classical trimer modes and excitation locations, we can now decrease the gap sizes into the subnanometer size regime by using the focused electron beam. Concurrently, we can collect EELS data on the modal evolution

DOI: 10.1021/acsnano.5b06738
ACS Nano 2016, 10, 1346−1354

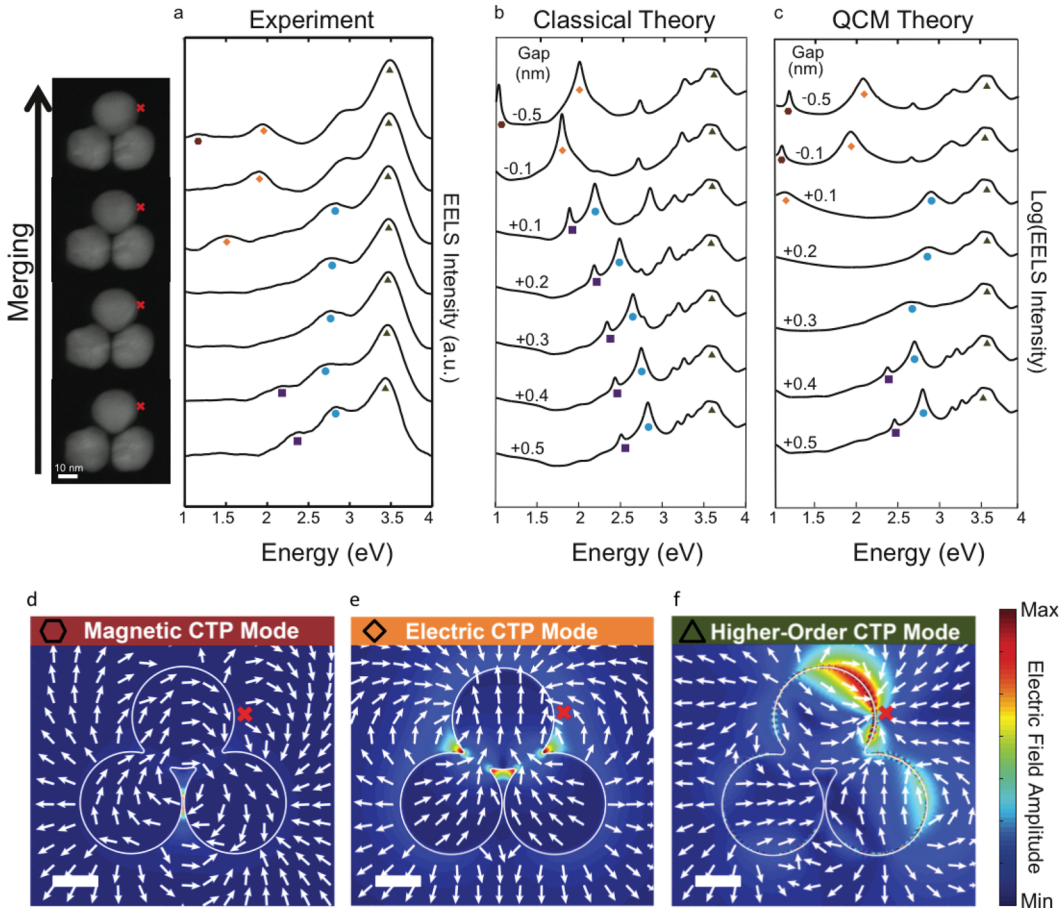

Figure 3. Spectral series comparing the plasmonic mode evolution in experimental EELS, classical theory, and quantum-corrected model (QCM) simulations as the particles merge (a–c). The spectra are accompanied by classical theoretical NF maps for the most relevant post merging modes (d–f). The trimer is excited with the electron beam in the edge position (red X's < 1 nm from the top particle) and proceeds to merge at the two top junctions. Experimental EELS data is systematically collected as the two junctions' gap sizes decrease and the prominent resonant modes are monitored, including magnetic (purple square), electric bonding (blue circle), higher-order modes (green triangle), electric charge transfer (orange rhombus) and magnetic charge transfer (brown hexagon). While all three spectral sets agree for merging separations ≥0.4 and <0 nm, only the QCM theory predicts the experimental trends at the smallest gaps. Further experimental and simulation details can be found in Methods.

while the trimer dimensions are altered. Our observations, described below, indicate the emergence of nonclassical plasmonic behavior for a select set of trimer modes, while others maintain purely classical behavior.

An example isosceles trimer merging and modal evolution sequence is depicted in Figure 3a. Starting with the trimer from Figure 2d, the electron beam is directed at the edge excitation location, causing the trimer to transform from three separated nanospheres (bottom) to a single merged entity with two physical junctions. This combination of excitation position and merging configuration supports both electric and magnetic modes before and after physical particle contact. In particular, experimental spectra show three peaks at 2.4 eV (purple square), 2.8 eV (blue circle), and 3.5 eV (green triangle) for ∼0.5 nm separations that evolve into two resonances as the lowest energy peak diminishes prior to particle contact. Then, as a physical connection forms, new, lower-energy resonances appear, including a strong peak initially at 1.5 eV (orange rhombus) that proceeds to blueshift during merging, as well as the emergence of a weaker peak at ∼1 eV (brown hexagon).

To understand the nature of the evolving plasmonic modes, we first compare our results to classical simulations, shown in Figure 3b. According to classical predictions, as the top two merging junctions' interparticle distances decrease from 0.5 to 0.1 nm, the trimer's magnetic mode (purple square) should continue to shift to lower energies and intensify, while the electric bonding mode (blue circle) should also redshift. Meanwhile, the dominant higher-order resonances at 3.5 eV should remain at constant energy throughout the merging process.

Once the particles touch (separation distances ≤0 nm), classical simulations predict that the bonding electric and magnetic modes disappear. Simultaneously, new modes emerge, as electrons can freely move between particles through a physical connection. At the lowest energies (∼1 eV), a new magnetic charge transfer plasmon (mCTP) mode appears (brown hexagon) with circulating displacement currents but only one interparticle gap instead of the original three (Figure 3d). An electric charge transfer plasmon (CTP)[56] mode also emerges and intensifies at ∼2 eV (orange rhombus), indicating that electrons can freely move between the particles through a physical connection, as seen in Figure 3e. As the nanospheres continue to merge (with negative separation distances), this electric CTP mode becomes stronger and blueshifts. Finally, the higher-order gap modes evolve into higher-order electric CTP modes (Figure 3f), which also have resonance frequencies

DOI: 10.1021/acsnano.5b06738
ACS Nano 2016, 10, 1346–1354

that remain unaltered at 3.5 eV (green triangle). For a detailed description of the modal evolution in the classical regime see Supporting Information Figure 2.

When panels a and b in Figure 3 are compared, it can be seen that the classical simulations display close correspondence with experimental EELS data for separation distances ≥0.4 and ≤0 nm. Both sets initially display the three primary resonances—magnetic, electric bonding, and higher-order—with the first two showing a slight redshift as the separation distance decreases. After contact, both simulation and experiment indicate the emergence of new electric CTP and mCTP modes at low energies.

For gap sizes between 0 and 0.4 nm, however, notable differences become apparent. In particular, the magnetic and electric bonding modes in the experimental data do not continue to redshift, as classical predictions would suggest. Instead, the magnetic mode becomes quenched, making it no longer visible at the smallest distances. The electric bonding mode also dampens and the resonance appears to blueshift prior to the particles coming into contact.

To understand this divergent behavior at Ångström-length scales, a quantum model becomes necessary. Previously, *ab initio* density functional theory models have provided a good point of comparison for dimer systems.[14,57,58] These models, however, have been computationally limited to relatively small systems, such as two 4 nm diameter Na spheres with ∼2000 conduction electrons.[57] To model the trimer composed of 25 nm-diameter silver particles in this study, over 1 million conduction electrons would need to be simulated.

Therefore, we apply a recently developed quantum-modified electrodynamic approach called the quantum-corrected model (QCM).[15] This strategy incorporates a quantum-modified treatment of the interparticle gap region conductivity in a classical simulation, accounting for the electron tunneling current between particles at optical frequencies. As tunneling probability is dependent on gap size, the interparticle junction is discretized into cylindric shells corresponding to different separation lengths and modeled with appropriate electron conductivities (σ_g). These, in turn, are used to calculate the permittivities of the gaps (ε_g).

The QCM has been benchmarked against Time-Dependent Density Functional Theory (TDDFT) calculations, indicating that it accurately describes the physics of the high frequency tunneling conductivity in small dimer systems. Moreover, it has been used to predict the behavior of larger, two-particle plasmonic systems.[15,16] Here, the QCM is employed to study the more complex nature of merging trimers[59] (additional details can be found in Methods).

At interparticle separations ≥0.4 and ≤0 nm, QCM simulations show close correspondence to both classical prediction trends and experimental data. Within the smallest gap region, however, it diverges from the classical model and follows a similar spectral evolution as the experimental STEM-EELS collections. As was observed in the experimental spectra, the magnetic and electric bonding resonances do not continue to redshift. Instead, the magnetic mode becomes quenched and the electric bonding resonance dampens and transforms into a higher-order charge transfer plasmon mode, which blueshifts prior to the particles touching. Similar electric mode phenomena have been predicted for dimers in the quantum regime.[15] Finally, the QCM simulations predict that the low-energy electric CTP emerges at +0.1 nm, before the particles physically come into contact. This feature has been reported in dimers[17] and is generated when the quantum tunneling probability is sufficiently high to facilitate interparticle conductivity.[56] This QCM prediction agrees well with the appearance of the CTP mode at lower energies in the experimental data.

To better illustrate the evolution of the magnetic and electric resonances at these Ångström-scale separation distances, Figure 4 shows the distribution of electric and magnetic field amplitudes and electric field directions for the relevant modes as the gap sizes diminish. The first column plots the magnetic field amplitude of the premerge magnetic mode, while the second column shows the electric field amplitude of the electric bonding mode. Rows 1 and 2 correspond to separation distances of 0.4 and 0.3 nm, before and after reaching the quantum tunneling threshold, respectively.

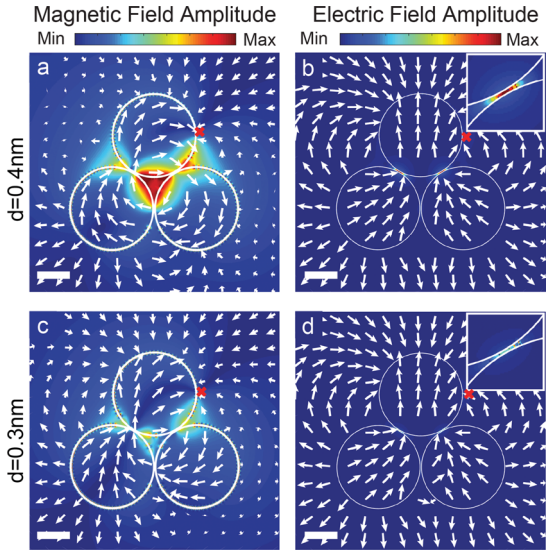

Figure 4. Electric and magnetic simulated field maps before and after the onset of quantum tunneling. Quantum-corrected model simulations of 25 nm-diameter silver nanosphere trimers with edge excitation (red X's) are generated at 0.4 nm gap distances (a and b), outside the quantum regime, and at 0.3 nm gap distances (c and d), where quantum tunneling is substantially stronger. As indicated by the electric field direction arrows, the magnetic mode is displayed at left (a and c), while the electric bonding mode is shown at right (b and d). The insets in b and d display a zoomed view of the electric fields in the gap regions. The quantum effects at the smaller separation distances result in a significant decrease in the magnetic and electric field amplitude for their corresponding modes. All scale bars equal 10 nm.

For d = 0.4 nm (Figure 4a,b), quantum tunneling still does not substantially impact the response of the system, and both electric and magnetic modes present the expected classical bonding behavior. The magnetic mode (Figure 4a) generates a strong magnetic field at the center of the system as a result of the circulating displacement currents across the three particle loop. The electric dipole mode instead presents intense electric fields at the particle gaps as a result of the strong coupling between the modes of the individual particles.

In contrast, the d = 0.3 nm separation distance (Figure 4c,d) is sufficiently small to allow a high-frequency tunneling current between the particles to be established. To use a circuit model analogy, at this threshold, the gap impedance acquires an increasingly resistive character (from the electron tunneling).

DOI: 10.1021/acsnano.5b06738
ACS Nano 2016, 10, 1346−1354

Further, the capacitive bonding nature of the modes loses strength, resulting in the damping and quenching of the bonding electric and magnetic modes. Consequently, the magnetic field amplitude map (Figure 4c) indicates a substantial drop in the magnetic field concentration at the center of the particle loop, and the electric fields in the interparticle gaps are similarly reduced (Figure 4d).

While the magnetic mode and the bonding electric mode display distinct nonclassical behavior, other plasmonic modes are not equally affected by quantum phenomena in the sub-nm regime. This contrast is seen when a trimer is excited through the center gap and the three particles symmetrically merge (all connections occurring simultaneously). The dark mode resonance, as seen in Figure 5a, initially occurs at 3.5 eV with 0.5 nm gap size and remains constant throughout the entire particle convergence.

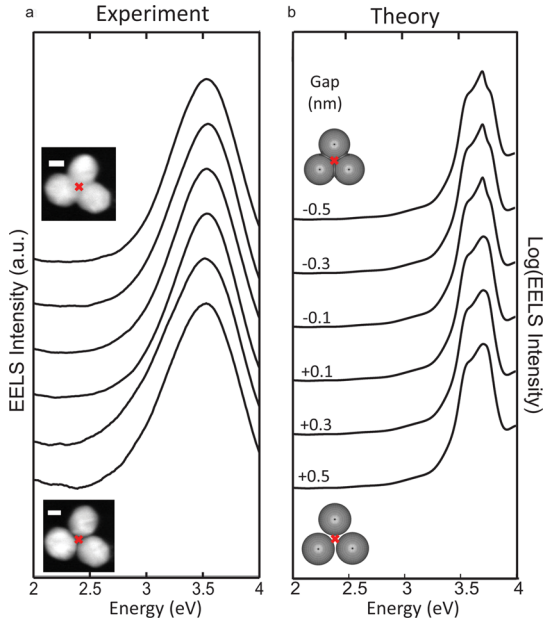

Figure 5. Spectral series comparing experimental EELS and classical simulations for a merging trimer with center excitation. The beam positions are indicated by red X's. Both experimental (a) and classical simulations (b) indicate a dominant peak that remains at a consistent energy throughout the merging process. All scale bars equal 10 nm.

Classical simulations (Figure 5b) are performed for comparison with experiment. Both reveal virtually identical resonance energy trends with separation distance, as the dark gap mode evolves into a dark merged trimer mode with similar field orientation (see Supporting Information Figure 3). This similarity between experimental data and classical simulations indicates that quantum effects do not influence the dark mode resonance behavior, even at the smallest interparticle dimensions.

Why does the dark mode behavior remain consistent between experiment and classical theory while the magnetic and bonding electric gap modes show substantial differences? This discrepancy is likely caused by the orientation of electric fields and charge distribution at the junctions; in the magnetic and electric bonding modes, charges with opposite polarity are induced at the interparticle interfaces, creating a strong local field through the gap and further facilitating electron tunneling between the nanospheres. The radially symmetric dark mode, in contrast, has identical charge polarity at the junctions, reducing the electric field and hindering electron transport between particles. For this distribution of induced charges, applying the quantum corrected model to the interparticle regions yields a gap permittivity equal to that of vacuum. Consequently, no tunneling occurs and the dark mode spectral evolution is identical to the trends determined through classical simulations. Note that this result should also be applicable to other dark modes of metamolecule assemblies, including the antibonding longitudinal modes of nanoparticle dimers.

CONCLUSIONS

To summarize, we have employed STEM-EELS for sub-nanometer imaging, selective excitation of hybridized multimer modes, spectral analysis, and electron-beam manipulation of nanoparticles. Further, we theoretically analyzed the response of the system through quantum-corrected model simulations. Combined, these methods allow us to explore fundamental trimer modes and their progression for interparticle gap sizes in the subnanometer regime. Plasmonic mode evolution during merging reveals that classical electrodynamics correctly captures the behavior of certain cases (*e.g.*, radially symmetric dark mode), but is insufficient for others (*i.e.*, electric bonding and magnetic modes) in which quantum phenomena appear. These spectral features, including resonance quenching and relative blueshifting, provide strong indication of electron tunneling between particles. Consideration of quantum features will play an important role in the design of future multiparticle metamolecules with sub-nm gaps and support new interdisciplinary exploration bridging molecular electronics, nonlinear optics, and plasmonics.

METHODS

Chemicals and Synthesis. Silver nanospheres are synthesized with citrate ligands according to previously described methods.[42] In brief, silver nitrate (>99% Alfa Aesar) is reduced in water by a combination of trisodium citrate (MP Biomedicals) and tannic acid (J.T. Baker), the quantity of the latter controlling the particle size. In this experiment, a 40 mL aqueous solution of 0.74 mM $AgNO_3$ is heated to 60 °C under constant stirring. A 10 mL aqueous solution of 6.8 mM citrate and 6 μM tannic acid is then rapidly added. Both solutions are prepared with Milli-Q deionized water (18 MΩ cm^{-1}). After 3 min, the combined mixture is further heated to a vigorous boil for 20 min before finally being allowed to cool to room temperature.

To remove excess citrate and unreacted metal salts in solution, the nanospheres are centrifuged at 8000 rpm for 10 min and the concentrated pellet is filtered with a 0.2 μm pore filter (Pall Corp.). This results in limiting the nanosphere size distribution to 25 ± 2 nm.

The particles in the concentrated and filtered solution are then dropcast onto a 8 nm-thick SiO_2 transmission electron microscope (TEM) membrane (Ted Pella, Inc.), which provides a smooth, inert surface for extended particle observation and electron-beam-induced motion, while also being sufficiently thin to minimize background and signal attenuation. Before deposition, the substrate is plasma cleaned to remove organic contamination and render the membrane more hydrophilic to aid in particle attachment. Once dropcast, the sample solution is allowed to dry on the membrane, and during the process the particles self-assemble into multimer clusters composed of varying number of nanospheres. Included among these particle clusters are the equilateral triangle trimers that are the focus of this study. The trimer particles are separated internally by ~1 nm gaps owing to the citrate ligands on the surfaces. The coverage of the citrate is nevertheless sufficiently sparse that particles were capable of coalescing when induced to move under the electron beam and do not demonstrate any carbon contamination during exposure.

DOI: 10.1021/acsnano.5b06738
ACS Nano 2016, 10, 1346–1354

Electron Microscopy. An FEI Titan 80–300 environmental (scanning) TEM is operated at 300 kV for highest, aberration-corrected TEM imaging resolution (0.07 nm). Scanning TEM (STEM) and electron energy-loss spectroscopy (EELS) operation, however, use 80 kV excitation, as it increases the particles' scattering cross-section and enables, with the aid of a monochromator, a spectral resolution of 0.1 eV, based on the full width at half-maximum of the zero-loss peak (ZLP). A Gatan 966 Quantum spectrometer is used with an energy dispersion of 0.01 eV per channel. A 50 μm C3 aperture, camera length of 48 mm, and a spectrometer entrance aperture of 2.5 mm are used, resulting in a convergence semiangle of 8.7 mrad and a collection semiangle of 20.2 mrad. The spatial imaging resolution with the focused STEM probe is 0.5 nm.

EELS data is collected by focusing the STEM beam at either 1 nm from the top trimer particle (top edge for "vertex" excitation, right edge for "edge" excitation) or at the center of the gap between the three nanoparticles. These relative locations are demonstrated in Figure 2. Generally, 1600 acquisitions, each lasting 10 ms, are collected between STEM images; the short time durations of the individual acquisitions are necessary to prevent the saturation of the CCD detector by the dominant ZLP.

Particle coalescence is caused by the energy and electric fields of the electron beam during spectral acquisition. Since the surface ligand coverage of the nanospheres is reduced through the aforementioned cleaning procedures, the particles could merge through a combination of electron-beam-facilitated surface diffusion[46−49] and an induced dipole−dipole coupling caused by the passing electrons' electric field.[41,45] To maximize particle movement during spectral acquisition while minimizing perturbation during imaging, the current of the beam is modulated between 250 pA for the former and 50 pA for the latter.

To generate the experimental series during trimer particle merging in Figure 3, continuous recordings of EELS data are collected between the acquisitions of the four STEM images. During those interval periods, the plasmonic response of the system slowly evolves, so the data is subdivided into sections of >500 acquisitions which exhibit relative consistency in resonance energies. These aligned and summed spectral subdivisions are presented as the seven spectra in Figure 3a.

Boundary Element Method Simulations. The experimental data of this study is compared to numerical calculations using the Boundary Element Method.[53,54] In particular, we used the Metallic Nanoparticle Boundary Element Method MATLAB toolbox.[55] In our study, a three-dimensional implementation and electron beam excitation source are used, allowing a fully rigorous simulation of the nanoparticle system geometry. Silver nanospheres (25 nm-diameter) with empirical bulk dielectric functions[60] are used as the trimer components and the electron beam is placed to match the experimental methods.

The particles are simulated in free space (ε = 1) to reduce computational complexity, but in so doing, ignore the influence of the SiO_2 substrate. As a result, isolated 25 nm silver spheres resonate at 3.5 eV rather than the 3.35 eV observed experimentally. Heuristically, this 0.15 eV difference can be accounted for through the use of an effective medium of ε = 1.3, which is the weighted average of the permittivity of surrounding vacuum (ε = 1) and that of the membrane (ε = 2.1) using a 2-to-1 ratio.[61]

For the edge excitation, BEM classical simulations model the trimer from an interparticle gap size of +0.5 nm down to particle contact at 0 nm assuming that the particles approach each other in an isosceles-like configuration; the separation distance between the two lower particles is kept constant at 0.5 nm while the other two interparticle gaps sizes are reduced. After a physical connection is formed, the nanospheres are assumed to directly overlap with negative separation distances. A tangent toroidal surface (inner radius = 0.5 nm) is applied to reduce the sharpness of this contact and ease the convergence of the calculations. This approach has been used in previous studies to simplify particle merging evolution[14,62]

For the center excitation (Figure 5 and Supplemental Information Figure 3), the three particles are assumed to converge equilaterally. After the physical contact, the three nanospheres are modeled to directly overlap with negative separation distances. As in the previous case, a tangent surface has been used to avoid singularities and facilitate the convergence of the calculations.

The Quantum-Corrected Model (QCM) simulations were employed using the approach introduced in ref 15. The QCM defines an effective material to be inserted in the gap, characterized by a frequency-dependent classical conductivity σ_g (or equivalently, permittivity ε_g) chosen to mimic the charge transfer from quantum tunneling. σ_g is initially calculated for low energies and then properly extended to high frequencies, in good agreement with the results of TDDFT calculations. The effective conductivity σ_g varies exponentially as a function of the local distance between each pair of opposing points across the gap, as described in detail in ref 63. Once ε_g has been defined, the optical response of the whole system is obtained with the BEM. As the simulation solves Maxwell's equations based on a distribution of surface charges and currents rather than using spatially inhomogeneous volumes, we consider several shells with a particular σ_g corresponding to a local separation distance. The shells extend only through the region where the local distance is smaller than 0.5 nm, as the tunneling substantially diminishes for larger separations. We verified that three shells are sufficient to obtain converged results of the EELS spectra and the NF maps. In the QCM simulations, no tangent surface is required after contact in order to converge the calculations, as the presence of the distance-dependent effective medium avoids discontinuities. For overlapping particles, the negative interparticle separation distance is defined in classical calculations as the length between the center of the particles minus the sum of the adjacent two particles' radii. The QCM negative separation distances are equivalent to those of the classical model when the area of the particle contact junction necks are the same.

ASSOCIATED CONTENT

Supporting Information

The Supporting Information is available free of charge on the ACS Publications website at DOI: 10.1021/acsnano.5b06738.

Additional trimer simulation field maps in the classical regime (PDF)

AUTHOR INFORMATION

Corresponding Authors

*E-mail: aitzolgarcia@dipc.org.
*E-mail: jdionne@stanford.edu.

Author Contributions

⊥J.A.S. and A.G.-E. contributed equally to this work.

Notes

The authors declare no competing financial interest.

ACKNOWLEDGMENTS

We thank Hadiseh Alaeian and Andrei Borissov for insightful discussions. Use of the Stanford Nano Shared Facilities is appreciated. A.G.-E., G.A., R.E., and J.A acknowledge project FIS2013-41184-P of the Spanish Ministry of Economy and Competitiveness. J.A.S. and J.A.D. acknowledge funding from a Presidential Early Career Award administered through the Air Force Office of Scientific Research (FA9550-15-1-0006), as well as funding from a National Science Foundation CAREER Award (DMR-1151231). Electron spectroscopy was partially supported by the DOE 'Light-Material Interactions in Energy Conversion' Energy Frontier Research Center under Grant DE-SC0001293. A.G.-E. and R.E. received funding from the Fellows Gipuzkoa fellowship of the Gipuzkoako Foru Aldundia through the FEDER "Una Manera de hacer Europa".

DOI: 10.1021/acsnano.5b06738
ACS Nano 2016, 10, 1346−1354

REFERENCES

(1) Atwater, H. A.; Polman, A. Plasmonics for Improved Photovoltaic Devices. *Nat. Mater.* **2010**, *9*, 205−213.
(2) Brongersma, M. L.; Halas, N. J.; Nordlander, P. Plasmon-Induced Hot Carrier Science and Technology. *Nat. Nanotechnol.* **2015**, *10*, 25−34.
(3) Christopher, P.; Xin, H.; Linic, S. Visible-Light-Enhanced Catalytic Oxidation Reactions on Plasmonic Silver Nanostructures. *Nat. Chem.* **2011**, *3*, 467−472.
(4) Anker, J. N.; Hall, W. P.; Lyandres, O.; Shah, N. C.; Zhao, J.; Van Duyne, R. P. Biosensing with Plasmonic Nanosensors. *Nat. Mater.* **2008**, *7*, 442−453.
(5) Stiles, P. L.; Dieringer, J. A.; Shah, N. C.; Van Duyne, R. P. Surface-Enhanced Raman Spectroscopy. *Annu. Rev. Anal. Chem.* **2008**, *1*, 601−626.
(6) Adato, R.; Yanik, A. A.; Amsden, J. J.; Kaplan, D. L.; Omenetto, F. G.; Hong, M. K.; Erramilli, S.; Altug, H. Ultra-sensitive Vibrational Spectroscopy of Protein Monolayers with Plasmonic Nanoantenna Arrays. *Proc. Natl. Acad. Sci. U. S. A.* **2009**, *106*, 19227−19232.
(7) Bardhan, R.; Lal, S.; Joshi, A.; Halas, N. J. Theranostic Nanoshells: from Probe Design to Imaging and Treatment of Cancer. *Acc. Chem. Res.* **2011**, *44*, 936−946.
(8) Huang, X.; El-Sayed, M. A. Gold nanoparticles: Optical Properties and Implementations in Cancer Diagnosis and Photothermal Therapy. *J. Adv. Res.* **2010**, *1*, 13−28.
(9) Oulton, R. F.; Sorger, V. J.; Zentgraf, T.; Ma, R.-M.; Gladden, C.; Dai, L.; Bartal, G.; Zhang, X. Plasmon Lasers at Deep Subwavelength Scale. *Nature* **2009**, *461*, 629−632.
(10) Bergman, D.; Stockman, M. Surface Plasmon Amplification by Stimulated Emission of Radiation: Quantum Generation of Coherent Surface Plasmons in Nanosystems. *Phys. Rev. Lett.* **2003**, *90*, 027402.
(11) Baum, B.; Alaeian, H.; Dionne, J. A parity-time Symmetric Coherent Plasmonic Absorber-Amplifier. *J. Appl. Phys.* **2015**, *117*, 063106.
(12) Scholl, J. A.; Koh, A. L.; Dionne, J. A. Quantum Plasmon Resonances of Individual Metallic Nanoparticles. *Nature* **2012**, *483*, 421−427.
(13) Zuloaga, J.; Prodan, E.; Nordlander, P. Quantum Description of the Plasmon Resonances of a Nanoparticle dimer. *Nano Lett.* **2009**, *9*, 887−891.
(14) Scholl, J. A.; García-Etxarri, A.; Koh, A. L.; Dionne, J. A. Observation of Quantum Tunneling Between Two Plasmonic Nanoparticles. *Nano Lett.* **2013**, *13*, 564−569.
(15) Esteban, R.; Borisov, A. G.; Nordlander, P.; Aizpurua, J. Bridging Quantum and Classical Plasmonics with a Quantum-Corrected Model. *Nat. Commun.* **2012**, *3*, 825.
(16) Savage, K. J.; Hawkeye, M. M.; Esteban, R.; Borisov, A. G.; Aizpurua, J.; Baumberg, J. J. Revealing the Quantum Regime in Tunnelling Plasmonics. *Nature* **2012**, *491*, 574−577.
(17) Tan, S. F.; Wu, L.; Yang, J. K. W.; Bai, P.; Bosman, M.; Nijhuis, C. A. Quantum Plasmon Resonances Controlled by Molecular Tunnel Junctions. *Science* **2014**, *343*, 1496−1499.
(18) Hajisalem, G.; Nezami, M. S.; Gordon, R. Probing the Quantum Tunneling Limit of Plasmonic Enhancement by Third Harmonic Generation. *Nano Lett.* **2014**, *14*, 6651−6654.
(19) Wu, L.; Duan, H.; Bai, P.; Bosman, M.; Yang, J. K. W.; Li, E. Fowler-Nordheim Tunneling Induced Charge Transfer Plasmons Between Nearly Touching Nanoparticles. *ACS Nano* **2013**, *7*, 707−716.
(20) Zhu, W.; Crozier, K. B. Quantum Mechanical Limit to Plasmonic Enhancement as Observed by Surface-Enhanced Raman Scattering. *Nat. Commun.* **2014**, *5*, 5228.
(21) Cha, H.; Yoon, J. H.; Yoon, S. Probing Quantum Plasmon Coupling Using Gold Nanoparticle Dimers with Tunable Interparticle Distances Down to the Subnanometer Range. *ACS Nano* **2014**, *8*, 8554−8563.
(22) Merlein, J.; Kahl, M.; Zuschlag, A.; Sell, A.; Halm, A.; Boneberg, J.; Leiderer, P.; Leitenstorfer, A.; Bratschitsch, R. Nanomechanical Control of an Optical Antenna. *Nat. Photonics* **2008**, *2*, 230−233.
(23) Sheikholeslami, S. N.; García-Etxarri, A.; Dionne, J. A. Controlling the Interplay of Electric and Magnetic Modes *via* Fano-like Plasmon Resonances. *Nano Lett.* **2011**, *11*, 3927−3934.
(24) Nazir, A.; Panaro, S.; Zaccaria, R. P.; Liberale, C.; Angelis, F. D.; Toma, A. Fano Coil-Type Resonance for Magnetic Hot-Spot Generation. *Nano Lett.* **2014**, *14*, 3166−3171.
(25) Shafiei, F.; Monticone, F.; Le, K. Q.; Liu, X.-X.; Hartsfield, T.; Alù, A.; Li, X. A subwavelength plasmonic metamolecule exhibiting magnetic-based optical Fano resonance. *Nat. Nanotechnol.* **2013**, *8*, 95−99.
(26) García-Etxarri, A.; Dionne, J. A. Surface-Enhanced Circular Dichroism Spectroscopy Mediated by Nonchiral Nanoantennas. *Phys. Rev. B: Condens. Matter Mater. Phys.* **2013**, *87*, 235409.
(27) Fan, Z.; Zhang, H.; Govorov, A. O. Optical Properties of Chiral Plasmonic Tetramers: Circular Dichroism and Multipole Effects. *J. Phys. Chem. C* **2013**, *117*, 14770−14777.
(28) Shalaev, V. M.; Cai, W.; Chettiar, U. K.; Yuan, H.-K.; Sarychev, A. K.; Drachev, V. P.; Kildishev, A. V. Negative Index of Refraction in Optical Metamaterials. *Opt. Lett.* **2005**, *30*, 3356−3358.
(29) Enkrich, C.; Wegener, M.; Linden, S.; Burger, S.; Zschiedrich, L.; Schmidt, F.; Zhou, J. F.; Koschny, T.; Soukoulis, C. M. Magnetic Metamaterials at Telecommunication and Visible Frequencies. *Phys. Rev. Lett.* **2005**, *95*, 203901.
(30) Alu, A.; Engheta, N. The Quest for Magnetic Plasmons at Optical Frequencies. *Opt. Express* **2009**, *17*, 5723−5730.
(31) Vallecchi, A.; Albani, M.; Capolino, F. Effect of Irregularities of Nanosatellites Position and Size on Collective Electric and Magnetic Plasmonic Resonances in Spherical Nanoclusters. *Opt. Express* **2013**, *21*, 7667−7685.
(32) Atre, A. C.; García-Etxarri, A.; Alaeian, H.; Dionne, J. A. A Broadband Negative Index Metamaterial at Optical Frequencies. *Adv. Opt. Mater.* **2013**, *1*, 327−333.
(33) Gómez, D. E.; Teo, Z. Q.; Altissimo, M.; Davis, T. J.; Earl, S.; Roberts, A. The Dark Side of Plasmonics. *Nano Lett.* **2013**, *13*, 3722−3728.
(34) Baldi, A.; Narayan, T. C.; Koh, A. L.; Dionne, J. A. In Situ Detection of Hydrogen-Induced Phase Transitions in Individual Palladium Nanocrystals. *Nat. Mater.* **2014**, *13*, 1143−1148.
(35) Fan, J. A.; Wu, C.; Bao, K.; Bao, J.; Bardhan, R.; Halas, N. J.; Manoharan, V. N.; Nordlander, P.; Shvets, G.; Capasso, F. Self-Assembled Plasmonic Nanoparticle Clusters. *Science* **2010**, *328*, 1135−1138.
(36) Alegret, J.; Rindzevicius, T.; Pakizeh, T.; Alaverdyan, Y.; Gunnarsson, L.; Käll, M. Plasmonic Properties of Silver Trimers with Trigonal Symmetry Fabricated by Electron-Beam Lithography. *J. Phys. Chem. C* **2008**, *112*, 14313−14317.
(37) Urzhumov, Y. A.; Shvets, G.; Fan, J. A.; Capasso, F.; Brandl, D.; Nordlander, P. Plasmonic Nanoclusters: a Path Towards Negative-Index Metafluids. *Opt. Express* **2007**, *15*, 14129−14145.
(38) Brandl, D. W.; Mirin, N. A.; Nordlander, P. Plasmon Modes of Nanosphere Trimers and Quadrumers. *J. Phys. Chem. B* **2006**, *110*, 12302−12310.
(39) Chuntonov, L.; Haran, G. Trimeric Plasmonic Molecules: The Role of Symmetry. *Nano Lett.* **2011**, *11*, 2440−2445.
(40) Zohar, N.; Chuntonov, L.; Haran, G. The Simplest Plasmonic Molecules: Metal Nanoparticle Dimers and Trimers. *J. Photochem. Photobiol., C* **2014**, *21*, 26−39.
(41) Batson, P. E.; Reyes-Coronado, A.; Barrera, R. G.; Rivacoba, A.; Echenique, P. M.; Aizpurua, J. Plasmonic Nanobilliards: Controlling Nanoparticle Movement Using Forces Induced by Swift Electrons. *Nano Lett.* **2011**, *11*, 3388−3393.
(42) Dadosh, T. Synthesis of Uniform Silver Nanoparticles with a Controllable Size. *Mater. Lett.* **2009**, *63*, 2236−2238.
(43) Nelayah, J.; Kociak, M.; Stephan, O.; García de Abajo, F. J.; Tence, M.; Henrard, L.; Taverna, D.; Pastoriza-Santos, I.; Liz-Marzan, L. M.; Colliex, C. Mapping Surface Plasmons on a Single Metallic Nanoparticle. *Nat. Phys.* **2007**, *3*, 348−353.
(44) Koh, A. L.; Bao, K.; Khan, I.; Smith, W. E.; Kothleitner, G.; Nordlander, P.; Maier, S. A.; McComb, D. W. Electron Energy-Loss

DOI: 10.1021/acsnano.5b06738
ACS Nano 2016, 10, 1346−1354

Spectroscopy Silver Nanoparticles and Dimers: Influence of Beam Damage and Mapping of Dark Modes. *ACS Nano* **2009**, *3*, 3015−3022.
(45) Reyes-Coronado, A.; Barrera, R.; Batson, P.; Echenique, P.; Rivacoba, A.; Aizpurua, J. Electromagnetic Forces on Plasmonic Nanoparticles Induced by Fast Electron Beams. *Phys. Rev. B: Condens. Matter Mater. Phys.* **2010**, *82*, 235429.
(46) José-Yacaman, M.; Gutierrez-Wing, C.; Miki, M.; Yang, D.-Q.; Piyakis, K. N.; Sacher, E. Surface Diffusion and Coalescence of Mobile Metal Nanoparticles. *J. Phys. Chem. B* **2005**, *109*, 9703−9711.
(47) Chen, Y.; Palmer, R. E.; Wilcoxon, J. P. Sintering of Passivated Gold Nanoparticles under the Electron Beam. *Langmuir* **2006**, *22*, 2851−2855.
(48) Lim, T. H.; McCarthy, D.; Hendy, S. C.; Stevens, K. J.; Brown, S. A.; Tilley, R. D. Real-time TEM and Kinetic Monte Carlo Studies of the Coalescence of Decahedral Gold Nanoparticles. *ACS Nano* **2009**, *3*, 3809−3813.
(49) Asoro, M. A.; Kovar, D.; Shao-Horn, Y.; Allard, L. F.; Ferreira, P. J. Coalescence and sintering of Pt Nanoparticles: in Situ Observation by Aberration-Corrected HAADF STEM. *Nanotechnology* **2010**, *21*, 025701.
(50) Koh, A. L.; Fernández-Domínguez, A. I.; McComb, D. W.; Maier, S. A.; Yang, J. K. W. High-Resolution Mapping of Electron-Beam-Excited Plasmon Modes in Lithographically Defined Gold Nanostructures. *Nano Lett.* **2011**, *11*, 1323−1330.
(51) Ögüt, B.; Talebi, N.; Vogelgesang, R.; Sigle, W.; van Aken, P. A. Toroidal Plasmonic Eigenmodes in Oligomer Nanocavities for the Visible. *Nano Lett.* **2012**, *12*, 5239−5244.
(52) Cherqui, C.; Bigelow, N. W.; Vaschillo, A.; Goldwyn, H.; Masiello, D. J. Combined Tight-Binding and Numerical Electrodynamics Understanding of the STEM/EELS Magneto-optical Responses of Aromatic Plasmon-Supporting Metal Oligomers. *ACS Photonics* **2014**, *1*, 1013−1024.
(53) García de Abajo, F. J.; Howie, A. Relativistic Electron Energy Loss and Electron-Induced Photon Emission in Inhomogeneous Dielectrics. *Phys. Rev. Lett.* **1998**, *80*, 5180.
(54) García de Abajo, F. J.; Howie, A. Retarded Field Calculation of Electron Energy Loss in Inhomogeneous Dielectrics. *Phys. Rev. B: Condens. Matter Mater. Phys.* **2002**, *65*, 115418.
(55) Hohenester, U.; Trügler, A. MNPBEM - A Matlab Toolbox For The Simulation of Plasmonic Nanoparticles. *Comput. Phys. Commun.* **2012**, *183*, 370−381.
(56) Pérez-González, O.; Zabala, N.; Borisov, A. G.; Halas, N. J.; Nordlander, P.; Aizpurua, J. Optical Spectroscopy of Conductive Junctions in Plasmonic Cavities. *Nano Lett.* **2010**, *10*, 3090−3095.
(57) Marinica, D. C.; Kazansky, A. K.; Nordlander, P.; Aizpurua, J.; Borisov, A. G. Quantum plasmonics: Nonlinear Effects in the Field Enhancement of a Plasmonic Nanoparticle Dimer. *Nano Lett.* **2012**, *12*, 1333−1339.
(58) Barbry, M.; Koval, P.; Marchesin, F.; Esteban, R.; Borisov, A. G.; Aizpurua, J.; Sánchez-Portal, D. Atomistic Near-Field Nanoplasmonics: Reaching Atomic-Scale Resolution in Nanooptics. *Nano Lett.* **2015**, *15*, 3410−3419.
(59) Hohenester, U. Quantum Corrected Model for Plasmonic Nanoparticles: A Boundary Element Method Implementation. *Phys. Rev. B: Condens. Matter Mater. Phys.* **2015**, *91*, 205436.
(60) Johnson, P. B.; Christy, R. W. Optical Constants of the Noble Metals. *Phys. Rev. B* **1972**, *6*, 4370.
(61) Biteen, J.; Sweatlock, L.; Mertens, H.; Lewis, N.; Polman, A.; Atwater, H. Plasmon-Enhanced Photoluminescence of Silicon Quantum Dots: Simulation and Experiment. *J. Phys. Chem. C* **2007**, *111*, 13372−13377.
(62) Romero, I.; Aizpurua, J.; Bryant, G. W.; García De Abajo, F. J. Plasmons in Nearly Touching Metallic Nanoparticles: Singular Response in the Limit of Touching Dimers. *Opt. Express* **2006**, *14*, 9988−9999.
(63) Esteban, R.; Zugarramurdi, A.; Zhang, P.; Nordlander, P.; García-Vidal, F. J.; Borisov, A. G.; Aizpurua, J. A Classical Treatment of Optical Tunneling in Plasmonic Gaps: Extending the Quantum Corrected Model to Practical Situations. *Faraday Discuss.* **2015**, *178*, 151−183.

DOI: 10.1021/acsnano.5b06738
ACS Nano 2016, 10, 1346−1354